frontiers | Frontiers in Immunology

TYPE Original Research
PUBLISHED 22 October 2025
DOI 10.3389/fimmu.2025.1665200

Check for updates

OPEN ACCESS

EDITED BY
Yi Liu,
Stanford University, United States

REVIEWED BY
Tingting Pan,
Shanghai Jiao Tong University, China
Muhammad Daniyal Waheed,
Maroof International Hospital, Pakistan

*CORRESPONDENCE
Lihui Deng
denglihui@scu.edu.cn

†These authors have contributed equally to this work and share first authorship

RECEIVED 13 July 2025
ACCEPTED 07 October 2025
PUBLISHED 22 October 2025

CITATION
Wang X, Hu C, Liu T, Yang R, Shen Y, Zhang S, Deng L and Xia Q (2025) CD44 and CLDN3 as immune-metabolic regulators in acute pancreatitis: a multi-modal transcriptomics study and experimental validation. *Front. Immunol.* 16:1665200. doi: 10.3389/fimmu.2025.1665200

COPYRIGHT
© 2025 Wang, Hu, Liu, Yang, Shen, Zhang, Deng and Xia. This is an open-access article distributed under the terms of the Creative Commons Attribution License (CC BY). The use, distribution or reproduction in other forums is permitted, provided the original author(s) and the copyright owner(s) are credited and that the original publication in this journal is cited, in accordance with accepted academic practice. No use, distribution or reproduction is permitted which does not comply with these terms.

CD44 and CLDN3 as immune-metabolic regulators in acute pancreatitis: a multi-modal transcriptomics study and experimental validation

Xinwei Wang†, Cheng Hu†, Tian Liu, Rui Yang, Yuxin Shen, Shihang Zhang, Lihui Deng* and Qing Xia

West China Centre of Excellence for Pancreatitis, Institute of Integrated Traditional Chinese and Western Medicine, West China Hospital, Sichuan University, Chengdu, China

Acute pancreatitis (AP) is an inflammatory disorder of exocrine pancreas regulated by a complex interaction between injured pancreatic acinar cells and immune cells. Recent studies indicated the crucial role of glycolysis in regulating immune cell function and inflammation. Here, we identified 43 glycolysis-related differentially expressed genes (DEGs) from transcriptomic datasets (GSE65146 and GSE109227). Through three machine learning algorithms,Claudin-3 (CLDN3) and CD44 were identified as key glycolysis-related DEGs. Their significant upregulation was further validated in an independent dataset. Then, single-sample gene set enrichment analysis revealed CLDN3 and CD44 were significantly correlated with immune-related structural remodeling and immune infiltration patterns. Single-cell RNA-seq analysis from GSE279876 confirmed that CLDN3 was downregulated in acinar cells, while CD44 was enriched in ductal and immune cells. To validate these findings, we established an AP model by 10 hourly intraperitoneal injections of caerulein (100 μg/kg) combined with one injection of lipopolysaccharide (10mg/kg). We confirmed that CD44 was upregulated and primarily expressed in inflammatory cells in AP mice. Interestingly, while CLDN3 mRNA levels were increased, its protein expression was reduced. Immunohistochemistry further revealed a redistribution of CLDN3 from the apical membrane to the cytoplasm in the pancreas of AP mice. Our findings, for the first time, indicated that CD44 and CLDN3 were crucial biomarkers associated with immune-metabolic dysregulation between pancreatic acinar cells and immune cells. The results of this study showed the potential of these two biomarkers as therapeutic targets for AP.

KEYWORDS

acute pancreatitis, inflammation, glycolysis, metabolic disorder, immune cell infiltration, machine learning, cellular landscape

1 Introduction

Acute pancreatitis (AP) is one of the most common digestive disorders worldwide and imposes a growing global health burden (1, 2). Up to 20% of AP patients progress to severe acute pancreatitis, which is associated with a mortality rate of 25% to 35% (3). As the molecular mechanisms of AP remain poorly understood, there is a lack of reliable early biomarkers and targeted therapies.

The crosstalk between pancreatic acinar cells and immune cells drives the disease progression. Cumulative evidences demonstrate that AP is primarily initiated by the premature activation of digestive enzymes within acinar cells (4). The subsequent release of proinflammatory cytokines and chemokines from the damaged acinar cells recruits the immune cells to the pancreas (5–8). The local inflammatory response of the pancreas further drives aberrant activation of adaptive immune responses (9, 10) to exacerbate the inflammation, triggering systemic inflammatory response and multiple organ dysfunction. Recent advances (8, 11–17) in single-cell RNA sequencing (scRNA-seq) have provided valuable insights into the cellular heterogeneity and immunopathology of AP. These studies have identified distinct neutrophil (12, 18, 19) and macrophage subpopulations (20–22) and uncovered immune–stromal interactions (18, 19, 23, 24) that drive both local pancreatic injury and systemic complications, highlighting the pivotal role of immune remodeling in AP progression.

Glycolysis is a cytosolic metabolic pathway that generates a rapid source of energy in the form of adenosine 5'-triphosphate (ATP) and nicotinamide adenine dinucleotide from the conversion of glucose by a cascade of enzymatic reactions. Beyond its traditional role in the anaerobic production of ATP, recent studies (25–29) have revealed that glycolysis also functions as a multifaceted metabolic pathway and signaling hub, which plays a crucial role in regulating the functions of immune cells and inflammatory response. Activated immune cells, including macrophages, B cells, and T cells, undergo a metabolic shift towards glycolysis to fuel processes of cytokine secretion, proliferation, and migration (30). However, the roles of glycolysis in both signaling and metabolic processes in AP have previously been overlooked.

A better understanding of the underlying molecular mechanisms of glycolysis in AP is essential to identify the promising biomarkers and therapeutic strategies. This study aims to systematically identify crucial glycolysis-related differentially expressed genes (DEGs) in AP through integrative transcriptomic analysis, to explore their functional roles, regulatory mechanisms, and immunometabolic relevance, and to validate the findings in the experiments *in vivo*.

2 Materials and methods

2.1 Data acquisition, differential expression analysis, and functional enrichment analysis

All datasets were obtained from the Gene Expression Omnibus (https://www.ncbi.nlm.nih.gov/geo/). The microarray datasets GSE65146 and GSE109227, based on the GPL6246 platform, were used for transcriptome analysis of pancreatic tissues from AP and control mice. Batch effects were corrected, and DEGs between AP and CTRL were identified using the limma package in R (version 4.3.1). Genes were defined as differentially expressed if $|(\log FC)| > 1$ and adjusted P-value < 0.05. Principal component analysis (PCA) was conducted to assess sample clustering and to evaluate the effectiveness of batch effect correction. The datasets GSE169076 (GPL23479) and GSE298193 (GPL25947) served as independent external validation cohorts in this study. The single-cell RNA-seq dataset GSE279876 (GPL19057) was used for cell-level resolution analysis. Detailed dataset characteristics and group assignments are provided in Supplementary Table 1. To explore the biological functions and pathways associated with the DEGs, Gene Ontology (GO) enrichment and Kyoto Encyclopedia of Genes and Genomes (KEGG) pathway analyses were performed using the clusterProfiler package in R. Terms or pathways with a P-value < 0.05 were considered significantly enriched.The overall workflow of this study is illustrated in Figure 1.

2.2 Identification of the key glycolysis-related DEGs by machine-learning algorithms

Glycolysis-related genes were compiled from gene sets in the Molecular Signatures Database (https://www.gsea-msigdb.org/gsea/msigdb/). After harmonizing gene symbols and removing duplicates (Supplementary Table 2), Glycolysis-related genes were intersected with the DEGs identified in our dataset to create a subset for downstream analysis. Three complementary machine learning algorithms including LASSO regression, Boruta feature selection, and SVM-RFE. LASSO logistic regression was performed using the glmnet R package and 10-fold cross-validation to select features based on the optimal lambda values (lambda.min and lambda.1se). Boruta in the Boruta R package was utilized to assess feature importance over 50 iterations, and tentative features were refined using TentativeRoughFix(). SVM-RFE was conducted using the sigFeature package and a custom msvmRFE script with 10-fold cross-validation to select the most predictive genes iteratively. Final key genes were defined by the intersection of the results from all three methods and validated by ROC curve analysis in the validation dataset.

2.3 Gene set enrichment analysis

Gene Set Enrichment Analysis (GSEA) was performed using the "HALLMARK_GLYCOLYSIS" gene set obtained from the MSigDB database to explore the functional relevance of glycolysis-related phenotypes. The analysis was based on a ranked list of all expressed genes ordered by their differential expression statistics. GSEA was conducted using the clusterProfiler R package. Enrichment significance was evaluated by normalized enrichment scores (NES) and false discovery rate (FDR) values. To further

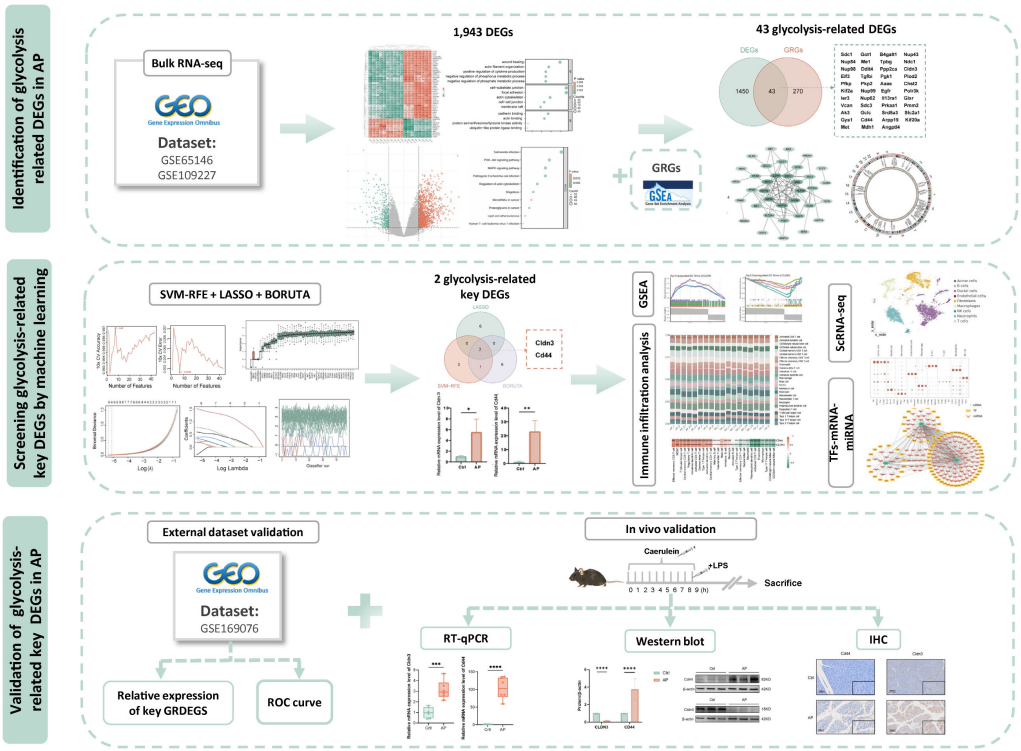

FIGURE 1
Study flowchart. DEGs, differentially expressed genes; AP, acute pancreatitis;GRGs, glycolysis related genes.

investigate the functional roles of key glycolysis-related DEGs, we performed GSEA on GO biological process terms for each gene individually. Genes with an absolute Spearman correlation ≥ 0.8 and p-value < 0.05 were selected for downstream analysis. Based on NES, the top five significantly enriched upregulated and downregulated GO biological processes were identified.

2.4 Protein-protein interaction network construction

Protein-protein interaction (PPI) networks were constructed to explore potential functional relationships among the glycolysis-related DEGs. Interaction data were obtained from the STRING database (https://cn.string-db.org/). Network visualization and analysis were carried out using Cytoscape (version 3.9.1). Hub genes were identified using the Maximal Clique Centrality (MCC) algorithm implemented in the CytoHubba plugin.

2.5 Single-cell RNA-seq analysis

ScRNA-seq data from control and AP samples (GSE298193) were processed using Scanpy (Python 3.8). Cells with < 200 genes, < 1,000 UMIs, or > 5% mitochondrial reads were excluded to remove low-quality or dying cells, and genes detected in fewer than 3 cells were removed to reduce noise. Putative doublets were identified using Scrublet (31), which simulates artificial doublets from the observed data and classifies cells based on transcriptome similarity. Scrublet was run separately for each sample with automatic thresholding, and cells predicted as doublets were removed before downstream analyses. Counts were normalized with a delta-method shifted log transformation, and the 2,000 most highly variable genes (HVG) were selected via the Pearson-residual method. PCA was performed on the scaled HVG matrix (top 50 PCs retained), and Leiden clustering was applied to the PCA space (resolution = 0.25). Cluster identities were assigned manually based on marker genes curated from CellMarker 2.0 (http://117.50.127.228/CellMarker/) and PanglaoDB (https://panglaodb.se/index.html). For visualization, a modified distance embedding was computed from the PCA space.

2.6 Immune cell infiltration analysis

The levels of immune cell infiltration were estimated using single-sample Gene Set Enrichment Analysis (ssGSEA) based on immune cell marker gene sets (32)(Supplementary Table 4). The enrichment scores were normalized to calculate the relative proportions of immune cells across samples. Differences in

immune infiltration between groups were evaluated using Student's t-test with multiple testing correction. Spearman correlation analysis was conducted to assess relationships among immune cell types as well as between immune infiltration and the key glycolysis-related DEGs. The results were visualized using heatmaps and boxplots to depict patterns of immune cell infiltration and their associations with core gene expression.

2.7 TFs-mRNA- miRNA regulatory network construction

NetworkAnalyst (https://www.networkanalyst.ca/) was used to generate the regulatory networks. TF-gene interactions were derived from ENCODE ChIP-seq data applying the BETA Minus algorithm with a peak intensity signal threshold of <500 and a predicted regulatory potential score of <1. MiRNA–gene interactions were obtained from miRTarBase v9.0. The integrated TF–miRNA–mRNA regulatory relationships were visualized using Cytoscape.

2.8 Experimental model, histological assessment

C57BL/6 mice (6–8 weeks old, 18–24 g weight) were purchased from Jiangsu GemPharmatech Co., Ltd. and housed under specific pathogen-free conditions (22–24 °C, 50–60% humidity, 12 h light/dark cycle). The AP model was induced by 10 hourly intraperitoneal (i.p.) injections of caerulein (100 μg/kg; Tocris, UK, Cat No.6264). Lipopolysaccharide (LPS; 10mg/kg; Sigma, USA, Cat No.2880) was administered (i.p.) immediately after the 10th caerulein injection. Mice were sacrificed 12 h after LPS injection. Amylase and lipase in serum and myeloperoxidase (MPO) activity in pancreatic and lung tissues were measured. Specimens of pancreatic and lung tissue were fixed in 10% formalin at room temperature for 24 hours and embedded in paraffin. Sections were stained with hematoxylin and eosin (H&E). Pathological severity was semi-quantitatively scored based on edema, inflammatory infiltration, and acinar necrosis, each rated on a 0–3 scale, as previously described (33, 34). Lung injury assessment was conducted by quantifying edema and the accumulation of inflammatory cells in 10 randomly selected fields per section at 100× magnification, as described in previous studies (33). Whole-slide imaging was performed using the Olympus SLIDEVIEW VS200 system (Olympus, Japan), and Fiji software was used for digital image analysis.

2.9 RT-qPCR analysis

Total RNA was extracted from pancreatic tissues using TRIzol reagent and was reverse transcribed into cDNA. qPCR was conducted using the Bio-Rad CFX96 Real-Time PCR System (Bio-Rad, USA) and SYBR Green Master Mix (Vazyme, China). Gene expression was quantified by the $2^{\wedge -\Delta\Delta Ct}$ method, normalized to 18S rRNA. Reagents and primer sequences are provided in the Supplementary Materials.

2.10 Western blot and immunohistochemistry

Western blot and immunohistochemistry (IHC) were performed to detect CLDN3 and CD44 expression in pancreatic tissues following standard protocols. The detailed methods were described in the Supplementary Materials.

2.11 Statistical analysis

Statistical analyses were conducted using R software (version 4.3.1) and GraphPad Prism 9.5 (GraphPad Software Inc., USA). Normally distributed data were presented as mean ± standard deviation and were analyzed using Student's t-test or one-way analysis of variance. Continuous data were analyzed using the Mann–Whitney U test. Correlations between variables were assessed using Pearson's or Spearman's correlation coefficients. All tests were two-tailed, and $p < 0.05$ was considered statistically significant.

3 Results

3.1 Identification of differential expression of genes of AP

After batch correction, normalized expression values were evenly distributed across the 10 Ctrl (Control) and 9 AP samples (Figure 2A; Supplementary Figure 1). Three-dimensional PCA confirmed a clear separation between AP and Ctrl samples (Figure 2B). Differential expression analysis using the limma package ($|\log_2 FC| \geq 1$, adjusted $P < 0.05$) identified 1,943 DEGs, comprising 1,156 upregulated and 787 downregulated genes (Figure 2C). Hierarchical clustering of the top 50 DEGs clearly distinguished AP from Ctrl samples, further supporting the differential expression patterns (Figure 2D). GO enrichment revealed that these DEGs are predominantly involved in biological processes (BP) such as wound healing, actin-filament organization, and positive regulation of cytokine production; associated with cellular components (CC) including the cell–substrate junction, focal adhesion, and actin cytoskeleton; and exhibited molecular functions (MF) such as cadherin binding, actin binding, and protein serine/threonine/tyrosine kinase activity (Figure 2E). KEGG pathway analysis showed significant enrichment in the PI3K–AKT, and MAPK signaling pathways (Figure 2F). These pathways reflect key pathophysiological features of AP, including immune activation, inflammatory signaling, cellular stress responses, and tissue repair mechanisms.

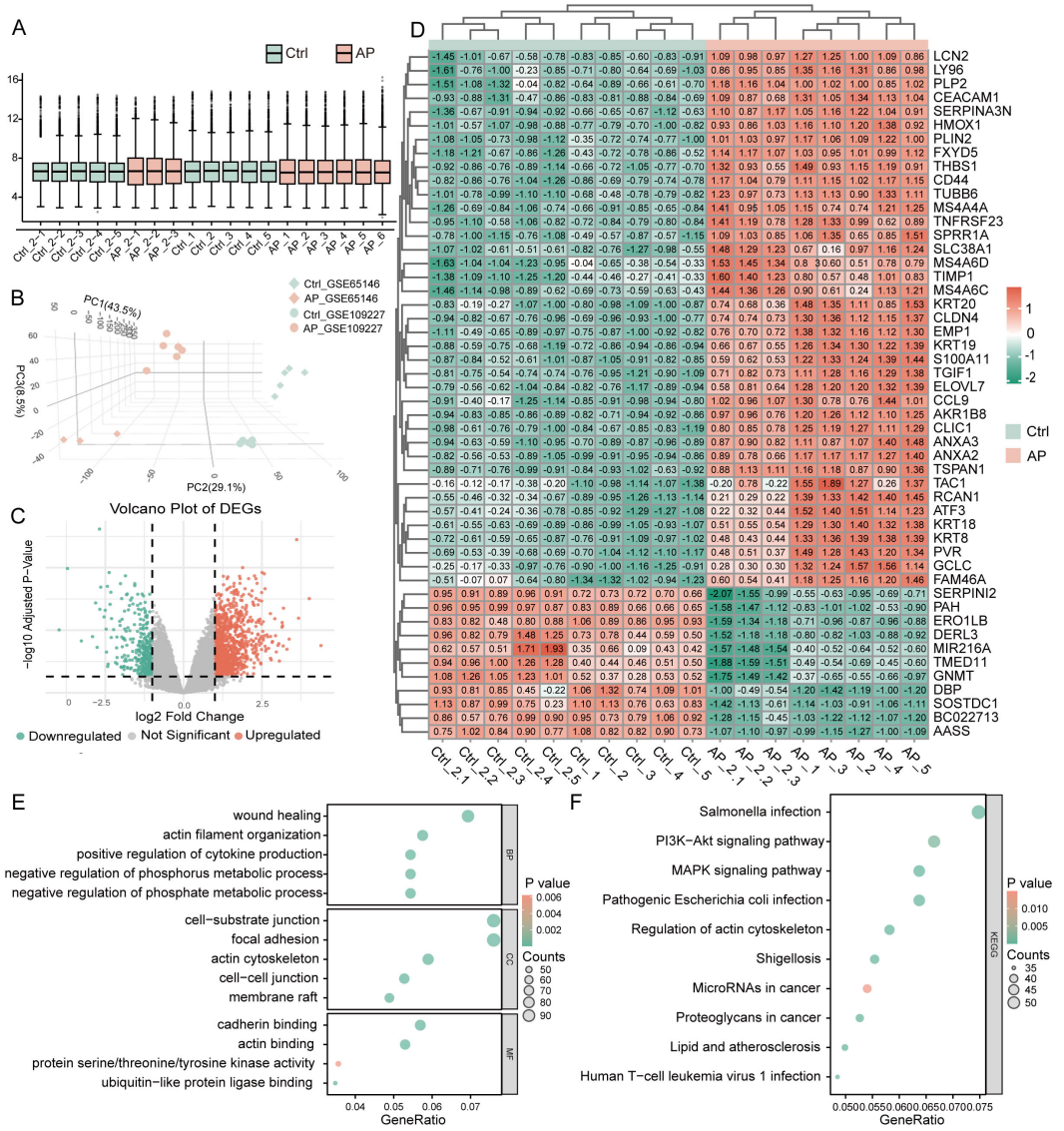

FIGURE 2
Identification and functional annotation of DEGs in AP. **(A)** Boxplot illustrating the distribution of gene expression values across all samples after batch effect correction. **(B)** The three-dimensional Principal Component Analysis plot shows AP and control sample clustering. **(C)** Volcano plot of DEGs between AP and control samples (threshold: $|\log_2 FC| \geq 1$, $P < 0.05$). **(D)** Heatmap of the top 50 DEGs ranked by statistical significance. **(E)** GO enrichment analysis of DEGs visualized using bubble plots, covering BP, CC, and MF categories. **(F)** KEGG pathway enrichment analysis of DEGs, shown as bubble plots. DEGs, differentially expressed genes; AP, acute pancreatitis; Ctrl, control; GO, Gene Ontology; BP, biological process; CC, cellular component; MF, molecular function; KEGG, Kyoto Encyclopedia of Genes and Genomes.

3.2 Glycolysis pathway enrichment and identification of glycolysis-related DEGs in AP

GSEA revealed significant enrichment of the glycolysis pathway in AP samples, with the NES of 2.48 and FDR below 0.25 (Figure 3A). By intersecting 1,483 DEGs with 313 glycolysis-related DEGs using a Venn diagram, 43 glycolysis-related DEGs were identified (Figure 3B). Boxplots comparing expression levels of the 43 glycolysis-related DEGs between AP and Ctrl groups showed distinct expression differences (Figure 3C). The chromosomal distribution revealed that glycolysis-related DEGs are clustered on chromosomes 5 and 6(Figure 3D, Supplementary Figure 2). A PPI network of the glycolysis-related DEGs was constructed based on the MCC algorithm to investigate potential interactions (Figure 3E, Supplementary Figure 3). Node colors represent MCC scores, highlighting hub genes within the network.

3.3 Identification of CD44 and CLDN3 as key glycolysis-related DEGs in AP

Glycolysis-related key DEGs of AP were identified by utilizing machine learning approaches. LASSO regression selected key

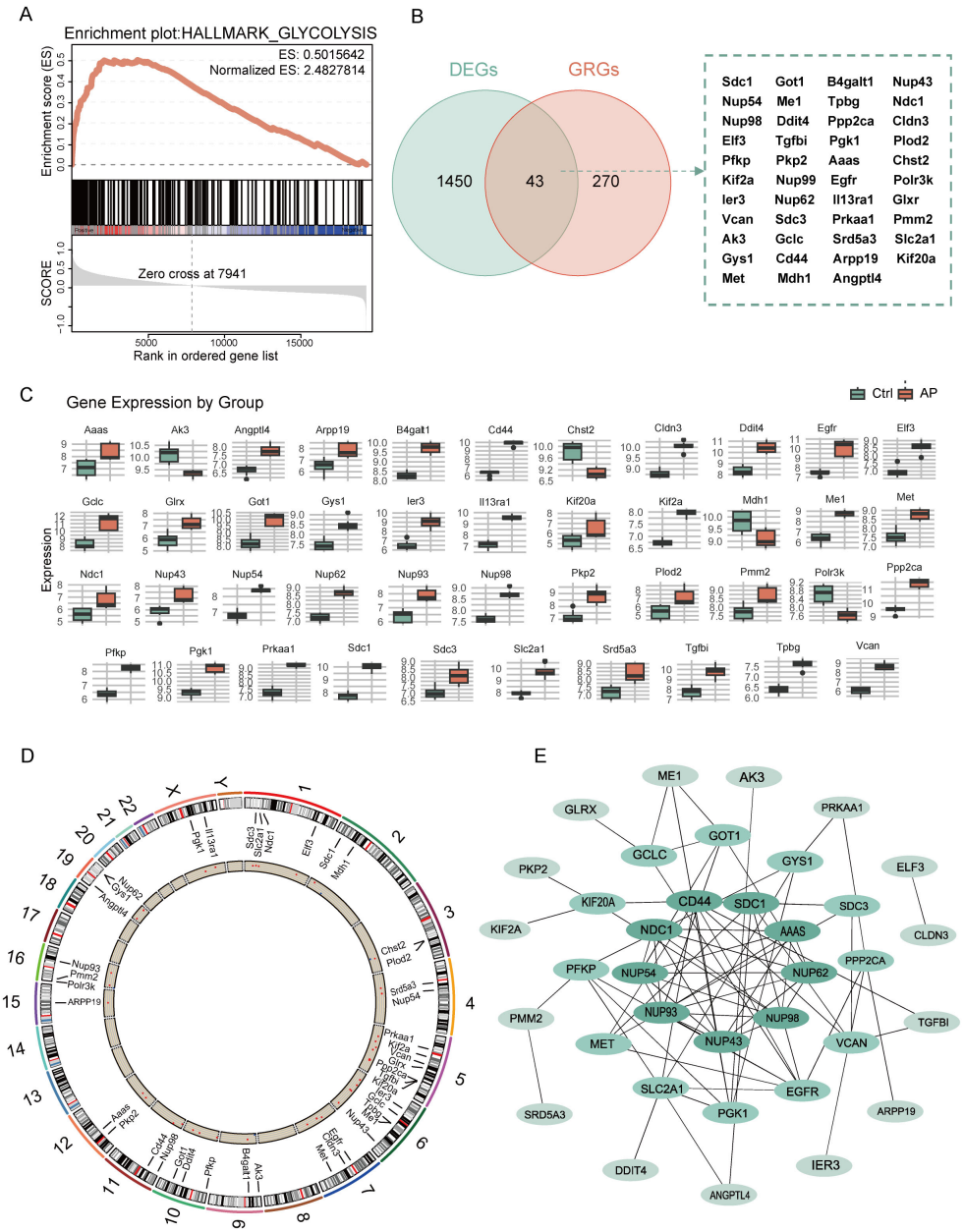

FIGURE 3
Analysis of glycolysis-related DEGs in AP. **(A)** GSEA enrichment plot showing the significant enrichment of the glycolysis pathway in AP. **(B)** Venn diagram showing the overlap between glycolysis-related genes and DEGs. **(C)** Boxplot depicting the relative expression levels of glycolysis-related DEGs between the control and AP samples. **(D)** Circular plot showing the chromosomal distribution of glycolysis-related DEGs. **(E)** PPI network of glycolysis-related DEGs, with node color intensity representing the MCC score. DEGs, differentially expressed genes; GRGs, glycolysis-related genes; ES, enrichment score; AP, acute pancreatitis; Ctrl, control; MCC, maximal clique centrality.

features with optimal lambda values determined by cross-validation (Figures 4A, B). SVM-RFE models were evaluated through accuracy and error rate analyses across multiple parameters (Figures 4C, D). Boruta feature selection further refined candidates by assessing feature importance and Z-scores over multiple iterations (Figures 4E, F). Integrating results from these methods identified 2 overlapping key glycolysis-related DEGs: Claudin-3 (CLDN3) and CD44 molecule (Figure 4G). Validation in an independent dataset confirmed significant upregulation of these genes in the AP samples (Figure 4H). In the validation datasets, ROC analysis yielded an Area Under the Curve (AUC) of 1.0 for both Cldn3 and Cd44 (Figure 4I, Supplementary Figure 4). Rather than indicating diagnostic applicability, these results primarily serve as evidence that the differential expression of these genes is robust and consistently observed across independent datasets.

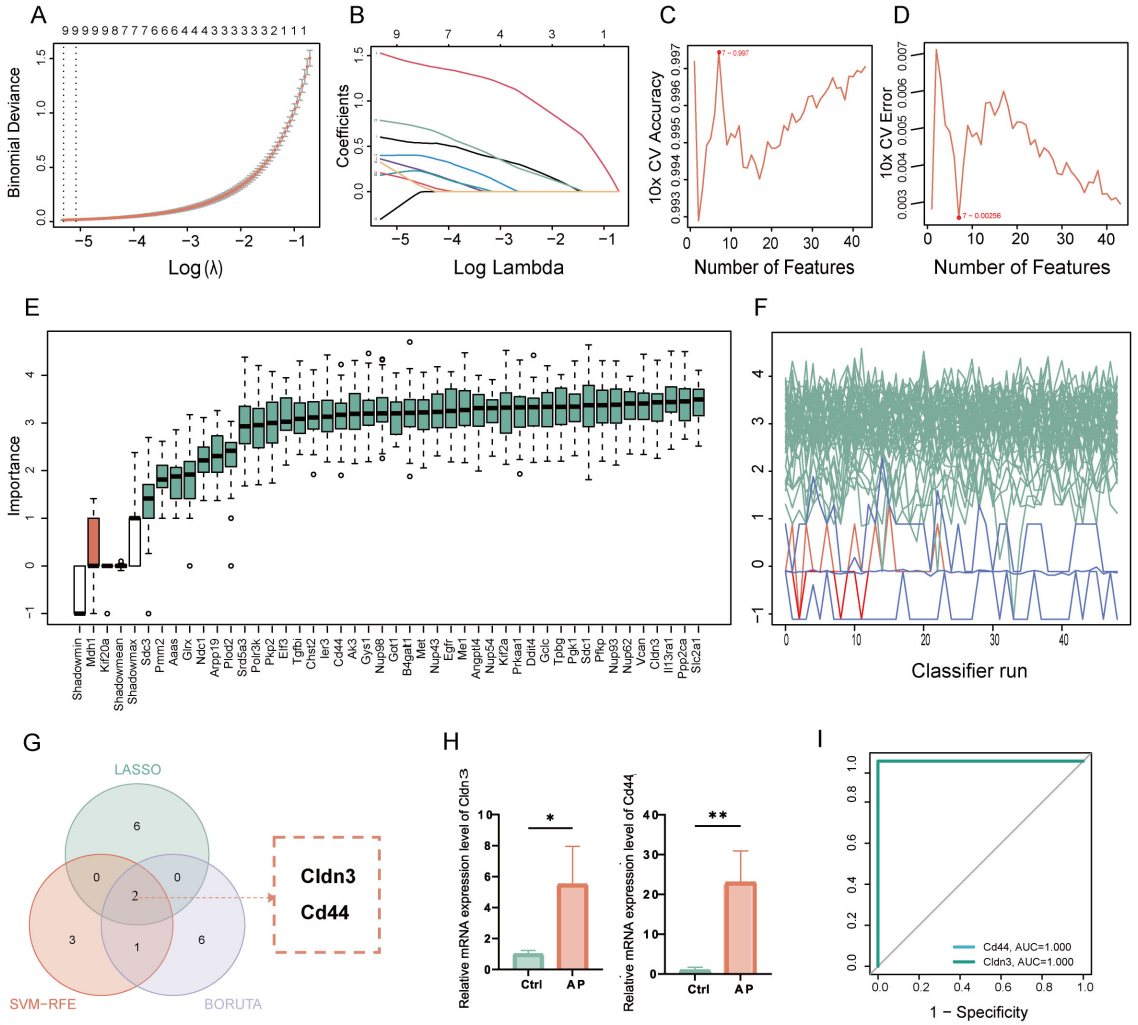

FIGURE 4
Identification and validation of key glycolysis-related DEGs through machine learning. **(A)** LASSO coefficient paths with vertical dashed lines marking lambda. min and lambda. 1se. **(B)** Mean cross-validation error across lambda values, highlighting the bias-variance trade-off. **(C)** Plot of SVM accuracy rates across different models. **(D)** Plot of SVM error rates across different models. **(E)** Boruta feature importance across iterations, with green for confirmed, red for rejected, and blue representing the minimum, average, and maximum Z-scores of shadow attributes. **(F)** Boruta feature Z-scores, with green for confirmed, red for rejected, and white boxes representing the minimum, average, and maximum Z-scores of shadow attributes. **(G)** Venn diagram showing the overlap of glycolysis-related key genes. **(H)** Relative mRNA expression of the key glycolysis-related DEGs in the validation set. **(I)** ROC curve of the glycolysis-related genes in the GSE169076 validation set. Ctrl, control; AP, acute pancreatitis. *p≤0.05,**p≤0.01.

3.4 GSEA on GO terms of CD44 and CLDN3

GSEA was performed on GO terms to explore the biological roles of CLDN3 and CD44 (Figure 5). The upregulated GO terms of these two genes were related to cell adhesion, extracellular vesicle formation, and RNA processing, which were essential for immune cell communication, migration, and activation. Conversely, the downregulated GO terms were enriched in sensory perception, ion transport, and transcription factor activity, which reflected a suppression of neuronal-like signaling pathways. These results suggest that CLDN3 and CD44 may contribute to immune-mediated structural remodeling and transcriptional regulation within the inflammatory microenvironment of AP.

3.5 Single-cell transcriptomic profile of CD44 and CLDN3

Single-cell quality control confirmed high data integrity (Figure 6A). Unsupervised clustering and marker-gene annotation identified the main cell populations of the pancreas—acinar, ductal, endothelial, fibroblast, B-cell, T-cell, NK-cell, macrophage, and neutrophil clusters (Figures 6B, C). There was an increasing

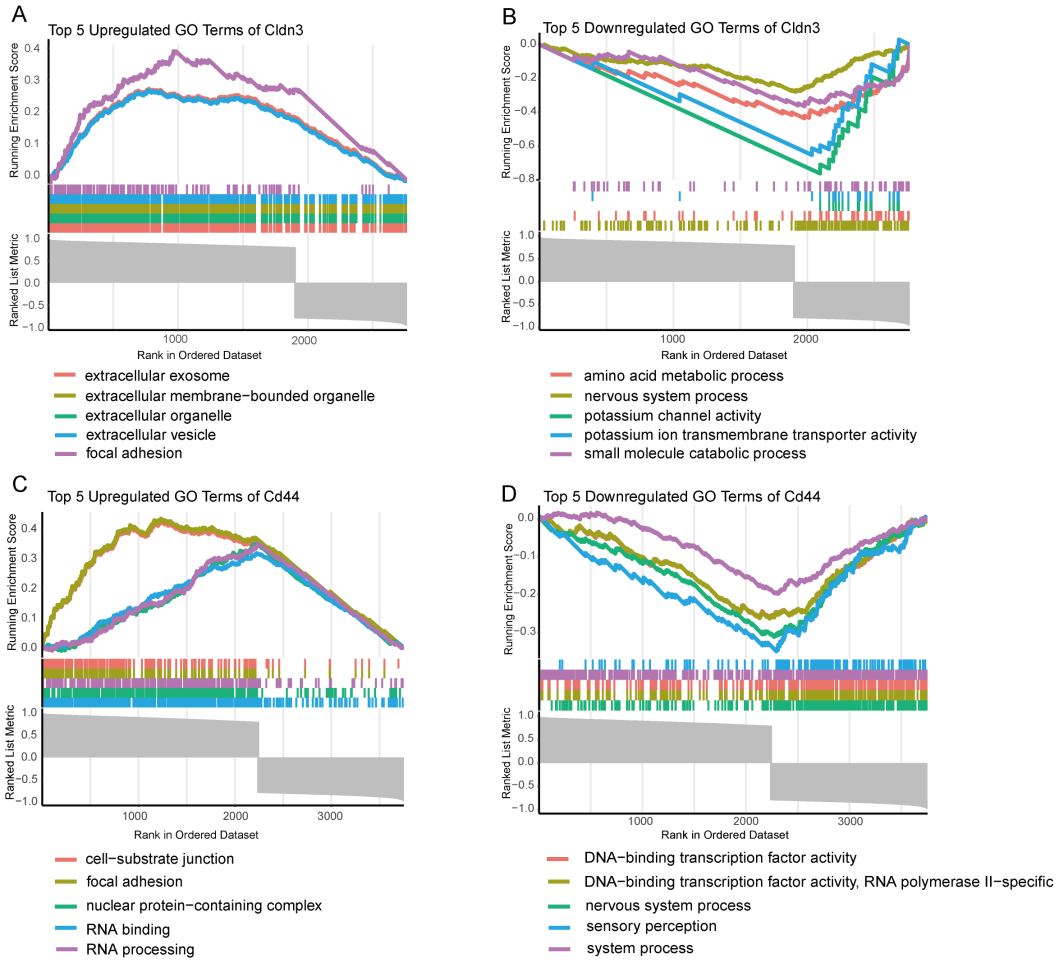

FIGURE 5
GSEA enrichment analysis of GO terms for key Genes. **(A)** Top 5 upregulated GO terms for CLDN3 based on GSEA analysis. **(B)** Top 5 downregulated GO terms for CLDN3 based on GSEA analysis. **(C)** Top 5 upregulated GO terms for CD44 based on GSEA analysis. **(D)** Top 5 downregulated GO terms for CD44 based on GSEA analysis.

number of immune cell populations and a remarkable loss of acinar cells in AP samples (Figures 6D, E). Cell-type–resolved mapping revealed the expression changes of glycolysis-related key genes in AP (Figures 6F-I). CD44 was enriched in both ductal and immune cells, which is consistent with the enhanced activation and migration of the immune cells. Notably, CLDN3 was significantly downregulated in acinar cells, indicating a disruption in epithelial integrity. This finding was inconsistent with bulk RNA-seq results, thereby prompting subsequent protein-level validation.

3.6 Immune infiltration and correlation analysis of CD44 and CLDN3 on ssGSEA

The ssGSEA analysis revealed distinct immune infiltration patterns of the pancreas in AP (Figure 7A). An increase in the expression of immune cell subsets was observed, indicating an alteration from a steady-state immune surveillance in normal status to an activated state. Correlation analysis among immune cells demonstrated the coordinated infiltration patterns, which indicated synergistic immune responses to the microenvironment in AP (Figure 7B). Notably, glycolysis-related key DEGs showed strong correlations with the majority of immune cells (Figure 7C, Supplementary Table 5), suggesting their broad regulatory roles in shaping the immune landscape during AP.

3.7 Prediction of TFs and miRNA of CD44 and CLDN3

To elucidate the upstream regulation of the glycolysis-related key DEGs, TFs, and miRNA networks were assembled from curated datasets (Figure 8). A total of 33 TFs were predicted to target these genes. At the post-transcriptional level, 138 miRNAs were identified to regulate the glycolysis-related key DEGs. Focusing on miRNAs with a degree of ≥1, 21 miRNAs were shared between CD44 and

10.3389/fimmu.2025.1665200

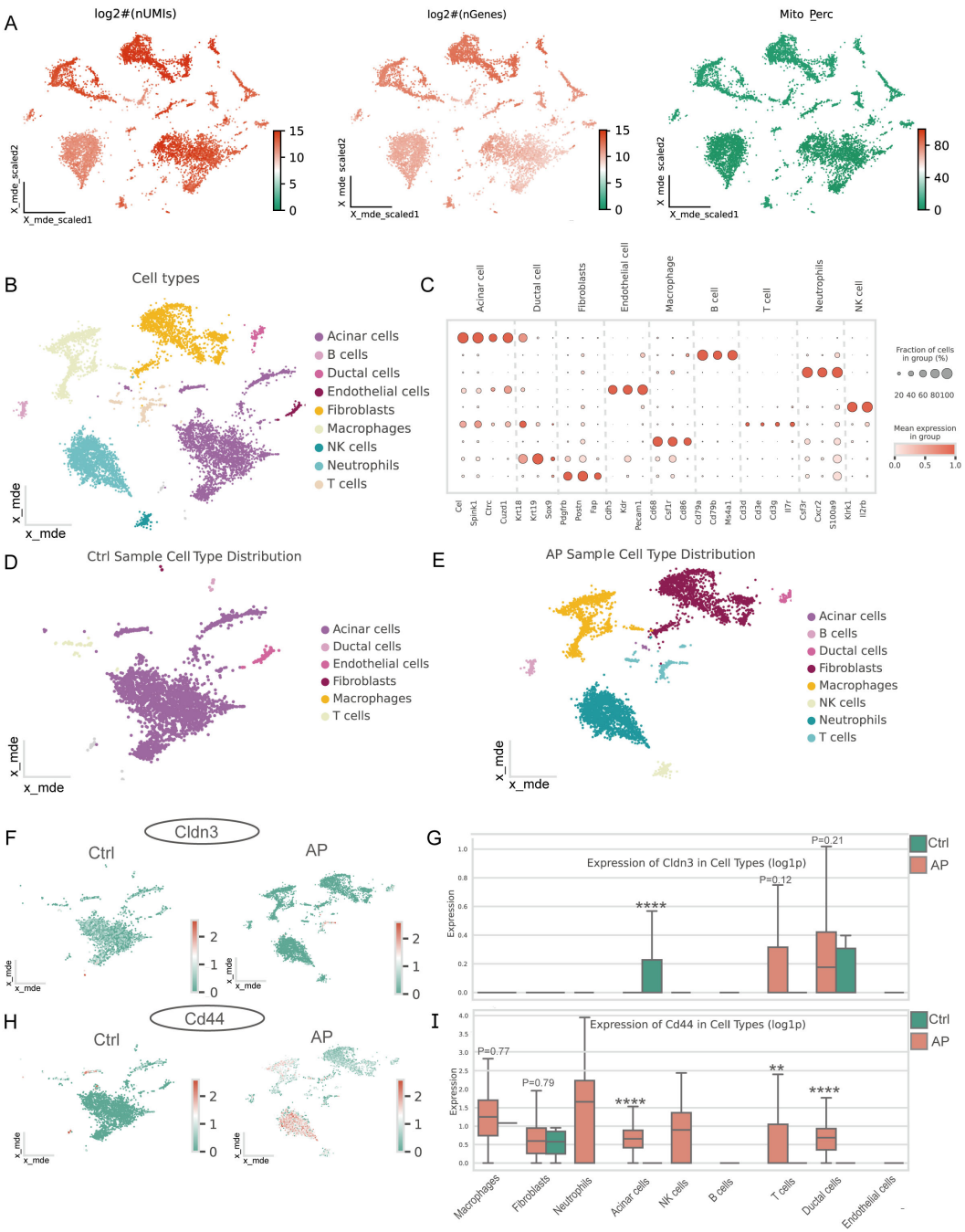

FIGURE 6
Single-cell characteristics of the pancreas in AP and features of glycolysis-related key DEGs. **(A)** Distribution of log-transformed UMI counts, gene counts, and mitochondrial gene expression percentage across cells, providing insights into the cellular quality of the dataset. **(B)** Major cell types in the pancreas. **(C)** Marker genes for different cell types. **(D)** Major cell types in the pancreas of the AP mice model. **(E)** Major cell types in the pancreas of healthy mice. **(F, H)** Spatial distribution of CLDN3 and CD44 in the pancreas from control and AP mice within the single-cell atlas. **(G, I)** Expression of CLDN3 and CD44 across major pancreatic cell types between AP and control.AP, acute pancreatitis; Ctrl, control. $^{**}p \leq 0.01$, $^{****}p \leq 0.0001$.

CLDN3(Supplementary Figure 6). Notably, SAP30, KDM5B, and PHF8 were identified as TFs regulating CD44, while TRIM24, SMARCA5, E2F5, and BCOR were predicted to regulate CLDN3. The identification of these shared miRNAs suggests post-transcriptional regulation of CD44 and CLDN3.

3.8 Validation of CD44 and CLDN3 in experimental AP model

To validate the bioinformatic findings, we established a mouse AP model by the combination of caerulein and LPS, as confirmed

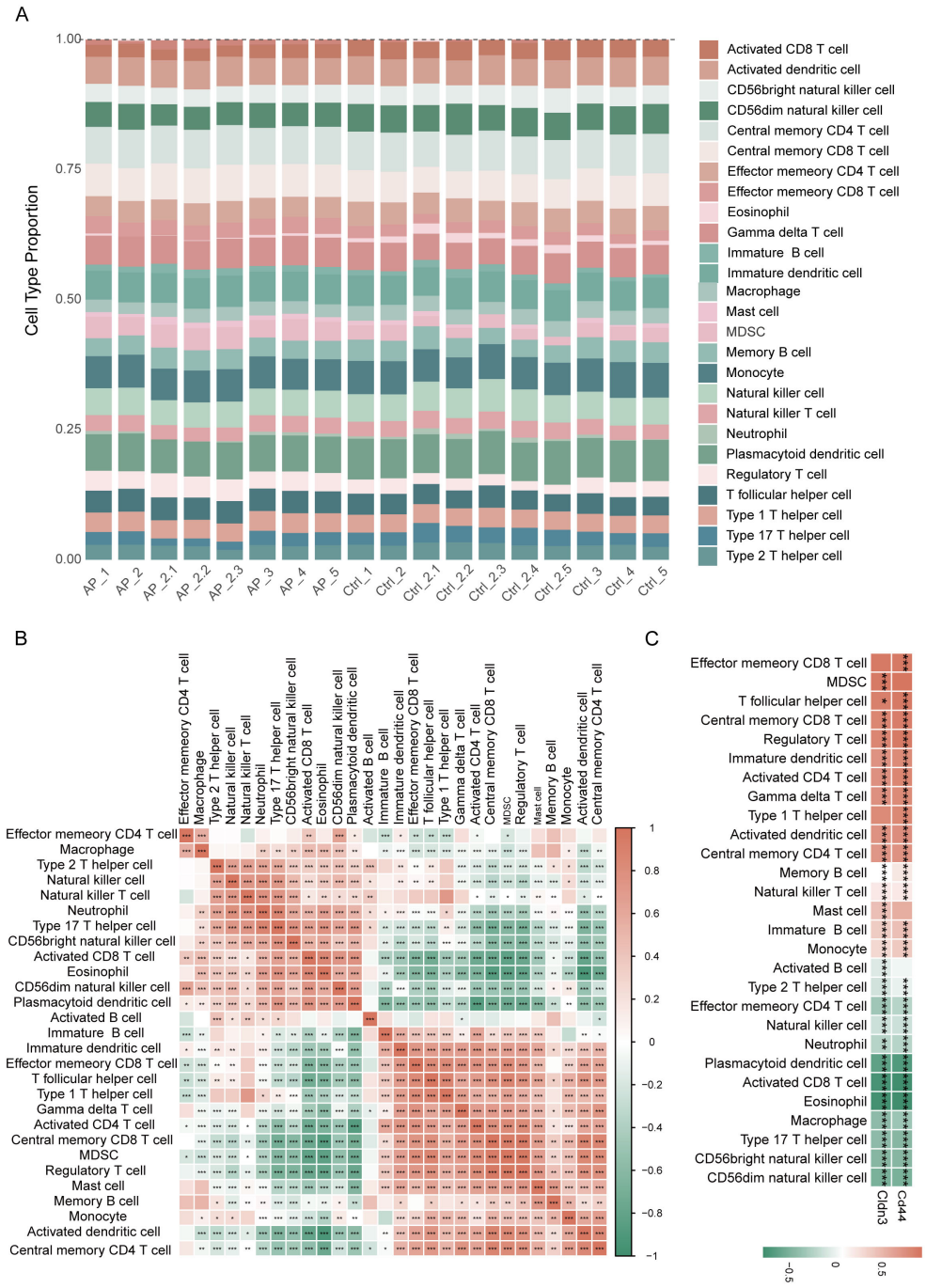

FIGURE 7
Immune infiltration analysis based on ssGSEA. **(A)** Proportions of immune cell types among different samples. **(B)** Heatmap depicting the correlation analysis of immune cells. **(C)** Heatmap showing the relationship between glycolysis-related key DEGs and immune cell infiltration. *p≤0.05,**p≤0.01, ***p≤0.001.

by serum amylase, lipase, and trypsin activity, and MPO activity in pancreatic tissue (Figures 9A-D), as well as H&E histopathological assessment (Figures 9F, G). The elevation of lung MPO activity and H&E scores indicated the involvement of the lungs (Figure 9E, H, I). We next assessed Cd44 and Cldn3 expression at both mRNA and protein levels by qPCR and western blotting (Figures 9J, K). Cd44 was upregulated at both transcriptional and protein levels in AP mice. Correspondingly, IHC staining showed that CD44 was predominantly expressed in inflammatory cells within pancreatic tissues of AP mice (Figure 9L). Interestingly, bulk qPCR indicated increased Cldn3 mRNA, whereas Western blotting revealed a marked protein reduction. This discrepancy likely reflects cell-type compositional shifts in AP, whereby increased Cldn3 expression in infiltrating immune and ductal cells masks its downregulation in acinar cells($p<0.0001$), as revealed by single-cell transcriptomics (Figure 6G). IHC further showed a

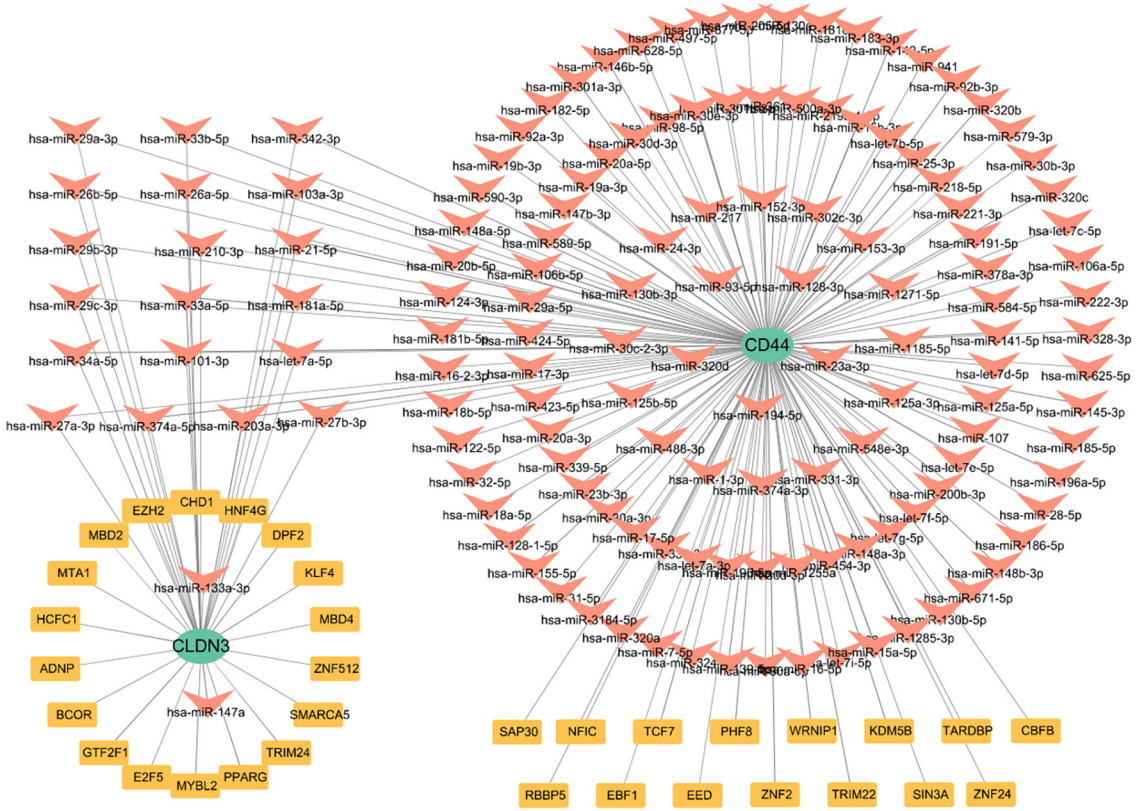

FIGURE 8
The TFs and miRNA regulatory network of CLDN3 and CD44.

redistribution of CLDN3 from acinar membranes in controls to diffuse cytoplasmic staining in AP mice(Figure 9M).

4 Discussion

To the best of our knowledge, this is the first study to investigate glycolysis and its immunoregulatory role in AP by integrating bulk and single-cell transcriptomic analyses, machine learning, and experimental validation. The results identify new insights of CD44 and CLDN3 into glycolysis-driven metabolic-immune mechanisms, and provide potential biomarkers and therapeutic targets for AP.

The cellular landscape in immunoregulation in AP is systematically constructed. Upregulation of glycolysis-related genes is consistent with immune and inflammatory mediators, highlighting the metabolic-immune interaction relationship in AP. Functional enrichment analyses of the DEGs and single-cell analysis reveal a complex interaction of immune cells infiltration and the loss of pancreatic acinar cells in AP, indicating tissue injury and immune activation during disease progression. Two immune cell clusters are shown in AP immune landscape: one cluster includes memory T cells, dendritic cells, and regulatory cells, which reflect a microenvironment in alleviating inflammation by immune regulation and suppression; the other cluster is consisted of activated B cells, natural killer cells, and effector cells, which represent a state of upregulated inflammatory response and innate immune activation. These findings underscore the complex immune regulatory mechanisms of the immune microenvironment in AP and suggest the potential of distinct immune cells as therapeutic strategies for AP. Significant enrichment of glycolytic pathways in AP tissues is confirmed by GSEA analysis. Key adhesion molecules and nuclear pore complex components are identified as central hubs, indicating the critical roles in immune cell adhesion and nuclear transport. Notably, CD44 and CLDN3 are identified via a combination of deep learning algorithms and validated in the experimental AP model.

CD44 is a cell surface adhesion molecule that plays extensive roles in the activation, recirculation, and homing of immune cells (35–39). It has been reported as a biomarker of cancer stem cells and facilitates metastasis, immune evasion, and therapeutic resistance (40–42). Recent studies demonstrate the role of CD44 in metabolic regulation, particularly in shifting glycolysis and oxidative phosphorylation (OXPHOS). CD44 modulates glycolytic metabolism by regulating key enzymes LDHA, LDHB, and PFKFB4 via HIF-1α and AMPK/mTOR signaling (43–47). In our study, CD44 is enriched in AP samples within pathways related to cell–matrix adhesion and RNA processing. In contrast, pathways associated with sensory perception and transcription factor activity are downregulated. These findings suggest that CD44 may

10.3389/fimmu.2025.1665200

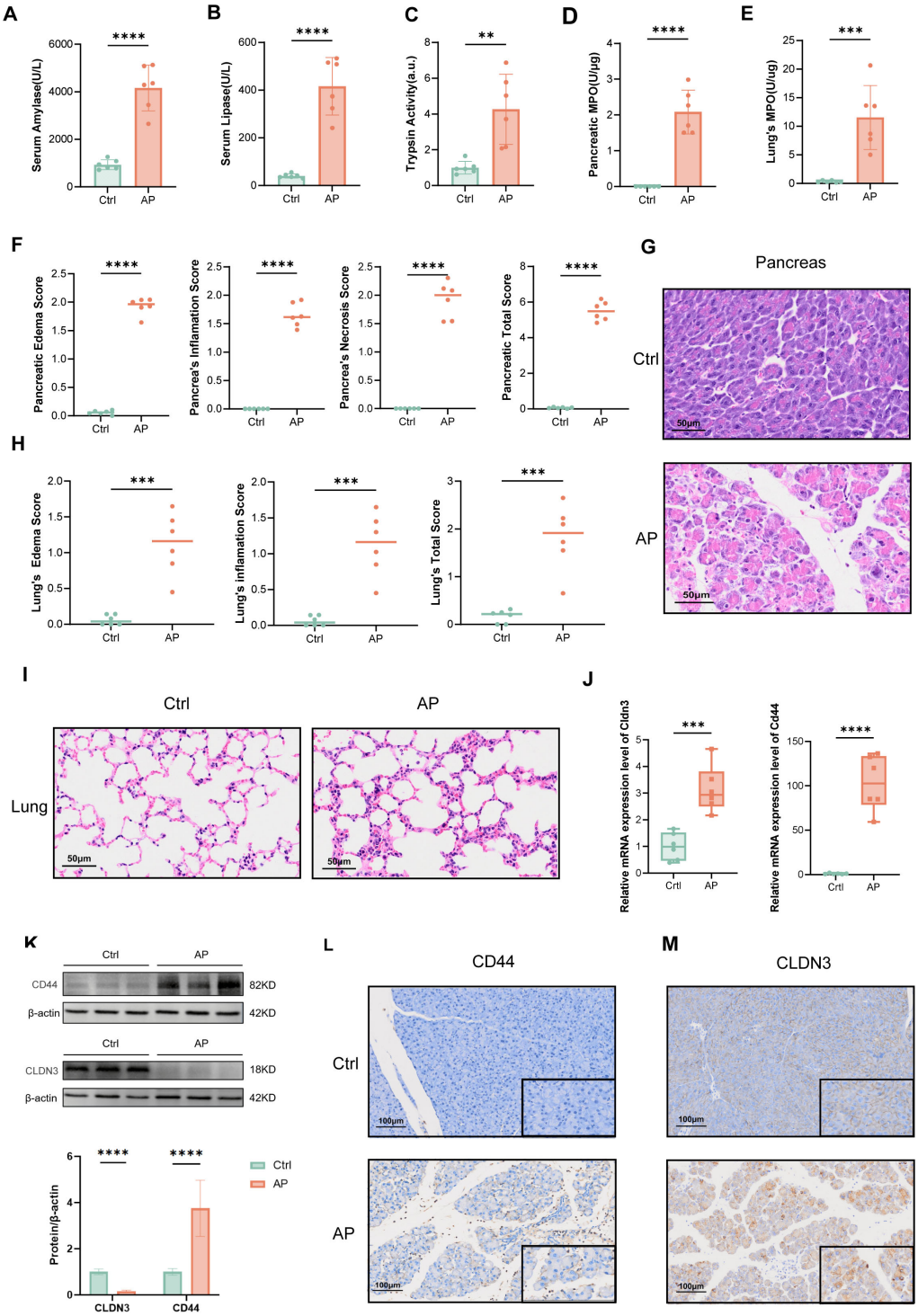

FIGURE 9
Validation of the AP model and expression of CLDN3 and CD44. (n = 6 biologically independent samples). Serum amylase levels. **(B)** Serum lipase levels. **(C)** Trypsin activity. **(D)** MPO activity in pancreatic tissue. **(E)** MPO activity in lung tissue. **(F)** Quantitative histopathological scores of the pancreas. **(G)** Representative H&E-stained images of pancreatic tissue from control and AP mice (200x). **(H)** Histopathological scores of the lung. **(I)** Representative H&E-stained images of lung tissue from control and AP mice (200x). **(J)** Relative mRNA expression levels of Cldn3 and Cd44 in pancreatic tissues. **(K)** Western blot analysis of CD44 and CLDN3 with quantification of band intensity normalized to β-actin. **(L, M)** IHC staining and semi-quantitative analysis of CLDN3 and CD44 in pancreatic tissues from control and AP mice (100x,400x). MPO, myeloperoxidase. **p≤0.01, ***p≤0.001,****p≤0.0001.

contribute to immune cell infiltration, post-transcriptional regulation, and cellular adaptation to inflammatory stress in AP. We identify CD44 as a crucial glycolysis-related DEG and validate its upregulated expression among a series of cells, including neutrophils, acinar cells, and ductal epithelial cells in AP samples. Correlation analysis between CLDN3 and CD44 with immune cell infiltration reveals significant associations with multiple immune cell types. These findings suggest that glycolysis–related key genes not only contribute to metabolic reprogramming but may also modulate immune cell infiltration, thereby influencing the immune microenvironment and pathological progression of AP.

CLDN3, which is highly expressed in epithelial and endothelial tissues (48, 49), is a crucial tight junction protein for maintaining epithelial barrier integrity. The dysregulation of CLDN3 has been implicated in cancer (50–55) and inflammatory diseases (56–58). Recent evidence (59–63) further suggests that CLDN3 expression is altered with elevated glycolytic activity in metabolic stress and tumors. In this study, we identified a discrepancy between the elevation of Cldn3 mRNA in bulk transcriptomic/qPCR data and the reduction of protein-level measurements by western blotting. Our ScRNA-seq transcriptomic data can help to resolve this paradox by revealing marked Cldn3 downregulation in acinar cells, alongside upregulation in ductal cells and T cells. During AP, massive immune cell infiltration and possible ductal hyperplasia can elevate the bulk mRNA signals despite acinar-specific suppression. However, because non-acinar cells contribute minimally to the total pancreatic protein pool, and inflammatory stress may promote CLDN3 internalization and degradation, the overall protein abundance still declines. IHC further revealed CLDN3 redistribution from the apical membrane to the cytoplasm in AP, a pattern consistent with tight junction disassembly and loss of epithelial polarity (64). Inflammatory cytokines such as TNF-α can trigger internalization of tight junction proteins, causing their removal from the membrane and cytoplasmic accumulation (65). In addition, disruption of polarity complexes such as PAR3/aPKC can facilitate endocytic uptake and lysosomal degradation of tight junction components (64, 66, 67). These inflammation-driven processes provide a mechanistic basis for the CLDN3 relocalization observed in AP. Collectively, these findings suggest that CLDN3, beyond its classical barrier role, participates in epithelial remodeling and immune modulation during AP.

Upstream regulators of glycolysis–related key genes are studied by constructing the TFs–mRNA–miRNA regulatory network. SAP30, KDM5B, and PHF8 are primarily epigenetic modifiers that may regulate CD44 expression via epigenetic regulation. TRIM24, SMARCA5, E2F5, and BCOR potentially regulate CLDN3 expression as transcriptional regulators and chromatin remodelers. Additionally, 21 shared miRNAs were computationally identified that may be involved in the post-transcriptional regulation of both CD44 and CLDN3, potentially linking these genes to immune modulation and metabolic processes in AP. These findings suggest a possible multilayered regulatory mechanism governing key glycolysis-related genes in AP.

This study explores the role of glycolysis in immune regulation in AP by using bulk transcriptomic, ScRNA-seq data, and experimental validation. However, there are several limitations. Firstly, it is limited by the exclusive use of a homogeneous mouse model and the absence of human patient data, which may introduce confounding factors and restrict the direct translational relevance of our findings. Future studies need to integrate the data from multiple animal models and clinical samples to validate the generalizability and clinical applicability of these observations. Secondly, the validation datasets yielded perfect AUC values for Cd44 and Cldn3. This phenomenon likely arises from intrinsic features of animal models, including controlled experimental conditions, synchronized sample collection, uniform disease induction, and inflammation-driven transcriptional changes, all of which can exaggerate group differences. Future validation in diverse clinical cohorts remains essential. Thirdly, although we systemically use GSEA, ScRNA-seq analysis, immune infiltration, and TFs-mRNA-miRNA analyses to explore potential regulatory mechanisms, this study remains preliminary. In-depth mechanistic studies are needed to elucidate the molecular mechanisms of glycolysis in regulating immune responses in AP.

5 Conclusion

This study identifies that CD44 and CLDN3 play crucial roles in metabolic regulation and immune modulation in AP, offering novel insights for biomarkers and therapeutic targets of the disease. Future researches are required to investigate the mechanisms underlying glycolysis-immune interactions of these genes in AP.

Data availability statement

The original contributions presented in the study are included in the article/Supplementary Material. Further inquiries can be directed to the corresponding author.

Ethics statement

The animal study was approved by Institutional Animal Care and Use Committee of West China Hospital, Sichuan University (No. 20250310019). The study was conducted in accordance with the local legislation and institutional requirements.

Author contributions

XW: Conceptualization, Data curation, Formal analysis, Visualization, Writing – original draft. CH: Conceptualization, Data curation, Formal analysis, Visualization, Writing – original draft. TL: Validation, Writing – original draft. RY: Validation, Writing – original draft. YS: Validation, Writing – original draft.

SZ: Validation, Writing – original draft. LD: Conceptualization, Funding acquisition, Supervision, Writing – review & editing. QX: Project administration, Supervision, Writing – review & editing.

Funding

The author(s) declare financial support was received for the research, and/or publication of this article. This work is supported by the National Natural Science Foundation of China (No. 82074230) and the Natural Science Foundation of Sichuan Province (Grant Nos. 2024NSFC0685 and 2025ZNSFSC0603).

Acknowledgments

We would like to express our acknowledgement to the staffs of Laboratory of Integrated Traditional Chinese and Western Medicine, West China Hospital of Sichuan University.

Conflict of interest

The authors declare that the research was conducted in the absence of any commercial or financial relationships that could be construed as a potential conflict of interest.

Generative AI statement

The author(s) declare that no Generative AI was used in the creation of this manuscript.

Any alternative text (alt text) provided alongside figures in this article has been generated by Frontiers with the support of artificial intelligence and reasonable efforts have been made to ensure accuracy, including review by the authors wherever possible. If you identify any issues, please contact us.

Publisher's note

All claims expressed in this article are solely those of the authors and do not necessarily represent those of their affiliated organizations, or those of the publisher, the editors and the reviewers. Any product that may be evaluated in this article, or claim that may be made by its manufacturer, is not guaranteed or endorsed by the publisher.

Supplementary material

The Supplementary Material for this article can be found online at: https://www.frontiersin.org/articles/10.3389/fimmu.2025.1665200/full#supplementary-material

References

1. Iannuzzi JP, King JA, Leong JH, Quan J, Windsor JW, Tanyingoh D, et al. Global incidence of acute pancreatitis is increasing over time: A systematic review and meta-analysis. *Gastroenterology*. (2022) 162:122–34. doi: 10.1053/j.gastro.2021.09.043

2. Xiao AY, Tan MLY, Wu LM, Asrani VM, Windsor JA, Yadav D, et al. Global incidence and mortality of pancreatic diseases: A systematic review, meta-analysis, and meta-regression of population-based cohort studies. *Lancet Gastroenterol Hepatol*. (2016) 1:45–55. doi: 10.1016/S2468-1253(16)30004-8

3. Boxhoorn L, Voermans RP, Bouwense SA, Bruno MJ, Verdonk RC, Boermeester MA, et al. Acute pancreatitis. *Lancet*. (2020) 396:726–34. doi: 10.1016/S0140-6736(20)31310-6

4. Mederos MA, Reber HA, Girgis MD. Acute pancreatitis: A review. *JAMA-J Am Med Assoc*. (2021) 325:382–90. doi: 10.1001/jama.2020.20317

5. Kang R, Lotze MT, Zeh HJ, Billiar TR, Tang D. Cell death and DAMPs in acute pancreatitis. *Mol Med*. (2014) 20:466–77. doi: 10.2119/molmed.2014.00117

6. Glaubitz J, Asgarbeik S, Lange R, Mazloum H, Elsheikh H, Weiss FU, et al. Immune response mechanisms in acute and chronic pancreatitis: Strategies for therapeutic intervention. *Front Immunol*. (2023) 14:1279539. doi: 10.3389/fimmu.2023.1279539

7. Fang Z, Li J, Cao F, Li F. Integration of scRNA-seq and bulk RNA-seq reveals molecular characterization of the immune microenvironment in acute pancreatitis. *Biomolecules*. (2023) 13:78. doi: 10.3390/biom13010078

8. Sun Z, Zhou R, Ning C, Zhu S, Li X, He Q, et al. scRNA-seq and bulk-seq identify novel markers associated with calcium regulation and immunomodulation in acute pancreatitis. *Pancreas*. (2025) 54:e512–23. doi: 10.1097/MPA.0000000000002421

9. Mititelu A, Grama A, Colceriu M-C, Pop TL. Overview of the cellular and immune mechanisms involved in acute pancreatitis: In search of new prognosis biomarkers. *Expert Rev Mol Med*. (2025) 27:e9. doi: 10.1017/erm.2024.40

10. Stojanovic B, Jovanovic IP, Stojanovic MD, Jovanovic M, Vekic B, Milosevic B, et al. The emerging roles of the adaptive immune response in acute pancreatitis. *Cells*. (2023) 12:1495. doi: 10.3390/cells12111495

11. Zhong L, Yang X, Shang Y, Yang Y, Li J, Liu S, et al. Exploring the pathogenesis, biomarkers, and potential drugs for type 2 diabetes mellitus and acute pancreatitis through a comprehensive bioinformatic analysis. *Front Endocrinol (Lausanne)*. (2024) 15:1405726. doi: 10.3389/fendo.2024.1405726

12. Zhang D, Wang X, Li W, Wan D, Zhou Y, Ma C, et al. A single-cell atlas-inspired hitchhiking therapeutic strategy for acute pancreatitis by restricting ROS in neutrophils. *Adv Mater*. (2025) 37:e2502200. doi: 10.1002/adma.202502200

13. Yang K, Xie R, Xiao G, Zhao Z, Ding M, Lin T, et al. The integration of single-cell and bulk RNA-seq atlas reveals ERS-mediated acinar cell damage in acute pancreatitis. *J Transl Med*. (2024) 22:346. doi: 10.1186/s12967-024-05156-0

14. Xie X, Wang Z, Zhang H, Lu J, Cao F, Li F. Identification of mitophagy-related biomarkers in severe acute pancreatitis: Integration of WGCNA, machine learning algorithms and scRNA-seq. *Front Immunol*. (2025) 16:1594085. doi: 10.3389/fimmu.2025.1594085

15. Tian S, Xin G, Zhang K, Wen A, Yu X, Ni C, et al. Eriodictyol from scutellariae barbata alleviates inflammation and necrosis via ZBP1-dependent signaling in acute pancreatitis. *Phytomedicine*. (2025) 145:156926. doi: 10.1016/j.phymed.2025.156926

16. Li B. From scRNA-seq to therapeutic targets: Unveiling the impact of activated mast cells on intestinal dysfunction in acute pancreatitis. *World J Gastroenterol*. (2025) 31:107865. doi: 10.3748/wjg.v31.i25.107865

17. Aney KJ, Jeong W-J, Vallejo AF, Burdziak C, Chen E, Wang A, et al. Novel approach for pancreas transcriptomics reveals the cellular landscape in homeostasis and acute pancreatitis. *Gastroenterology*. (2024) 166:1100–13. doi: 10.1053/j.gastro.2024.01.043

18. Wang Q, Zhang X, Han C, Lv Z, Zheng Y, Liu X, et al. Immunodynamic axis of fibroblast-driven neutrophil infiltration in acute pancreatitis: NF-κB-HIF-1α-CXCL1. *Cell Mol Biol Lett*. (2025) 30:57. doi: 10.1186/s11658-025-00734-6

19. Liu X, Zheng Y, Meng Z, Wang H, Zhang Y, Xue D. Gene regulation of neutrophils mediated liver and lung injury through NETosis in acute pancreatitis. *Inflammation*. (2025) 48:393–411. doi: 10.1007/s10753-024-02071-w

20. Lin S, Liang F, Chen C, Lin J, Wu Y, Hou Z, et al. Annexin A1 regulates inflammatory-immune response and reduces pancreatic and extra- pancreatic injury during severe acute pancreatitis. *Genes Immun*. (2025) 26:124–36. doi: 10.1038/s41435-025-00321-x

21. Shen Q, Wang S, Wu K, Wang L, Gong W, Lu G, et al. Identification of Grb2 protein as a potential mediator of macrophage activation in acute pancreatitis based on bioinformatics and experimental verification. *Front Immunol*. (2025) 16:1575880. doi: 10.3389/fimmu.2025.1575880

22. Wu Z, Wang S, Wu Z, Tao J, Li L, Zheng C, et al. Altered immune cell in human severe acute pancreatitis revealed by single-cell RNA sequencing. *Front Immunol*. (2024) 15:1354926. doi: 10.3389/fimmu.2024.1354926

23. Feng Y, Chen W, Chen J, Sun F, Kong F, Li L, et al. Dietary emulsifier carboxymethylcellulose-induced gut dysbiosis and SCFA reduction aggravate acute pancreatitis through classical monocyte activation. *Microbiome*. (2025) 13:83. doi: 10.1186/s40168-025-02074-1

24. Wei Z-X, Jiang S-H, Qi X-Y, Cheng Y-M, Liu Q, Hou X-Y, et al. scRNA-seq of the intestine reveals the key role of mast cells in early gut dysfunction associated with acute pancreatitis. *World J Gastroenterol*. (2025) 31:103094. doi: 10.3748/wjg.v31.i12.103094

25. Saaoud F, Liu L, Xu K, Cueto R, Shao Y, Lu Y, et al. Aorta- and liver-generated TMAO enhances trained immunity for increased inflammation via ER stress/mitochondrial ROS/glycolysis pathways. *JCI Insight*. (2023) 8:e158183. doi: 10.1172/jci.insight.158183

26. Zhang X, Liu J, Li X, Zheng G, Wang T, Sun H, et al. Blocking the HIF-1α/glycolysis axis inhibits allergic airway inflammation by reducing ILC2 metabolism and function. *Allergy*. (2025) 80:1309–34. doi: 10.1111/all.16361

27. Kwon H-K, Yu KE, Cahill SV, Alder KD, Dussik CM, Kim S-H, et al. Concurrent targeting of glycolysis in bacteria and host cell inflammation in septic arthritis. *EMBO Mol Med*. (2022) 14:e15284. doi: 10.15252/emmm.202115284

28. Xuan L, Ren L, Zhang W, Du P, Li B, An Z. Formaldehyde aggravates airway inflammation through induction of glycolysis in an experimental model of asthma exacerbated by lipopolysaccharide. *Sci Total Environ*. (2024) 912:168947. doi: 10.1016/j.scitotenv.2023.168947

29. Sánchez-Bayuela T, Peral-Rodrigo M, Parra-Izquierdo I, López J, Gómez C, Montero O, et al. Inflammation via JAK-STAT/HIF-1α drives metabolic changes in pentose phosphate pathway and glycolysis that support aortic valve cell calcification. *Arterioscler Thromb Vasc Biol*. (2025). doi: 10.1161/ATVBAHA.124.322375

30. Pająk B, Zieliński R, Priebe W. The impact of glycolysis and its inhibitors on the immune response to inflammation and autoimmunity. *Molecules*. (2024) 29:1298. doi: 10.3390/molecules29061298

31. Wolock SL, Lopez R, Klein AM. Scrublet: computational identification of cell doublets in single-cell transcriptomic data. *Cell Syst*. (2019) 8:281–291.e9. doi: 10.1016/j.cels.2018.11.005

32. Charoentong P, Finotello F, Angelova M, Mayer C, Efremova M, Rieder D, et al. Pan-cancer immunogenomic analyses reveal genotype-immunophenotype relationships and predictors of response to checkpoint blockade. *Cell Rep*. (2017) 18:248–62. doi: 10.1016/j.celrep.2016.12.019

33. Huang W, Cane MC, Mukherjee R, Szatmary P, Zhang X, Elliott V, et al. Caffeine protects against experimental acute pancreatitis by inhibition of inositol 1,4,5-trisphosphate receptor-mediated Ca2+ release. *Gut*. (2017) 66:301–13. doi: 10.1136/gutjnl-2015-309363

34. Wen Y, Li Y, Liu T, Huang L, Yao L, Deng D, et al. Chaiqin chengqi decoction treatment mitigates hypertriglyceridemia-associated acute pancreatitis by modulating liver-mediated glycerophospholipid metabolism. *Phytomedicine*. (2024) 134:155968. doi: 10.1016/j.phymed.2024.155968

35. Yanova M, Stepanova E, Maltseva D, Tonevitsky A. CD44 variant exons induce chemoresistance by modulating cell death pathways. *Front Cell Dev Biol*. (2025) 13:1508577. doi: 10.3389/fcell.2025.1508577

36. Skandalis SS. CD44 intracellular domain: A long tale of a short tail. *Cancers (Basel)*. (2023) 15:5041. doi: 10.3390/cancers15205041

37. Salathia S, Gigliobianco MR, Casadidio C, Di Martino P, Censi R. Hyaluronic acid-based nanosystems for CD44 mediated anti-inflammatory and antinociceptive activity. *Int J Mol Sci*. (2023) 24:7286. doi: 10.3390/ijms24087286

38. Inoue A, Ohnishi T, Nishikawa M, Ohtsuka Y, Kusakabe K, Yano H, et al. A narrative review on CD44's role in glioblastoma invasion, proliferation, and tumor recurrence. *Cancers (Basel)*. (2023) 15:4898. doi: 10.3390/cancers15194898

39. Cirillo N. The hyaluronan/CD44 axis: A double-edged sword in cancer. *Int J Mol Sci*. (2023) 24:15812. doi: 10.3390/ijms242115812

40. Ziranu P, Pretta A, Aimola V, Cau F, Mariani S, D'Agata AP, et al. CD44: A new prognostic marker in colorectal cancer? *Cancers (Basel)*. (2024) 16:1569. doi: 10.3390/cancers16081569

41. Wu S, Tan Y, Li F, Han Y, Zhang S, Lin X. CD44: A cancer stem cell marker and therapeutic target in leukemia treatment. *Front Immunol*. (2024) 15:1354992. doi: 10.3389/fimmu.2024.1354992

42. Sonnentag SJ, Ibrahim NSM, Orian-Rousseau V. CD44: A stemness driver, regulator, and marker-all in one? *Stem Cells*. (2024) 42:1031–9. doi: 10.1093/stmcls/sxae060

43. De Falco V, Tamburrino A, Ventre S, Castellone MD, Malek M, Manié SN, et al. CD44 proteolysis increases CREB phosphorylation and sustains proliferation of thyroid cancer cells. *Cancer Res*. (2012) 72:1449–58. doi: 10.1158/0008-5472.CAN-11-3320

44. Gao R, Li D, Xun J, Zhou W, Li J, Wang J, et al. CD44ICD promotes breast cancer stemness via PFKFB4-mediated glucose metabolism. *Theranostics*. (2018) 8:6248–62. doi: 10.7150/thno.28721

45. Semenza GL, Jiang BH, Leung SW, Passantino R, Concordet JP, Maire P, et al. Hypoxia response elements in the aldolase a, enolase 1, and lactate dehydrogenase a gene promoters contain essential binding sites for hypoxia-inducible factor 1. *J Biol Chem*. (1996) 271:32529–37. doi: 10.1074/jbc.271.51.32529

46. Tamada M, Nagano O, Tateyama S, Ohmura M, Yae T, Ishimoto T, et al. Modulation of glucose metabolism by CD44 contributes to antioxidant status and drug resistance in cancer cells. *Cancer Res*. (2012) 72:1438–48. doi: 10.1158/0008-5472.CAN-11-3024

47. Nam K, Oh S, Shin I. Ablation of CD44 induces glycolysis-to-oxidative phosphorylation transition via modulation of the c-src-akt-LKB1-AMPKα pathway. *Biochem J*. (2016) 473:3013–30. doi: 10.1042/BCJ20160613

48. Günzel D, Yu ASL. Claudins and the modulation of tight junction permeability. *Physiol Rev*. (2013) 93:525–69. doi: 10.1152/physrev.00019.2012

49. Nakamura S, Irie K, Tanaka H, Nishikawa K, Suzuki H, Saitoh Y, et al. Morphologic determinant of tight junctions revealed by claudin-3 structures. *Nat Commun*. (2019) 10:816. doi: 10.1038/s41467-019-08760-7

50. Yuan M, Chen X, Sun Y, Jiang L, Xia Z, Ye K, et al. ZDHHC12-mediated claudin-3 S-palmitoylation determines ovarian cancer progression. *Acta Pharm Sin B*. (2020) 10:1426–39. doi: 10.1016/j.apsb.2020.03.008

51. Luo M, Wang X, Yu G, Ji J, Li L, Song F. Development of a bispecific antibody-drug conjugate targeting EpCAM and CLDN3 for the treatment of multiple solid tumors. *Exp Hematol Oncol*. (2025) 14:33. doi: 10.1186/s40164-025-00624-9

52. Liu W, Kuai Y, Wang D, Chen J, Xiong F, Wu G, et al. PPM1G inhibits epithelial-mesenchymal transition in cholangiocarcinoma by catalyzing TET1 dephosphorylation for destabilization to impair its targeted demethylation of the CLDN3 promoter. *Adv Sci (Weinh)*. (2024) 11:e2407323. doi: 10.1002/advs.202407323

53. Jiang F, Li S, Wang X, Deng Y, Peng S. DPP10-AS1-mediated downregulation of MicroRNA-324-3p is conducive to the Malignancy of pancreatic cancer by enhancing CLDN3 expression. *Pancreas*. (2022) 51:1201–10. doi: 10.1097/MPA.0000000000002164

54. Büyücek S, Schraps N, Menz A, Lutz F, Chirico V, Viehweger F, et al. Prevalence and clinical significance of claudin-3 expression in cancer: A tissue microarray study on 14,966 tumor samples. *biomark Res*. (2024) 12:154. doi: 10.1186/s40364-024-00702-w

55. Zhao J, Ke J, Cao X, Li J, Gu M, Zhou X, et al. p38 MAPK–mediated upregulation of claudin-3 and claudin-4 by gemcitabine contributes to chemoresistance in ovarian cancer. *Int J Biochem Cell Biol*. (2025) 185:106805. doi: 10.1016/j.biocel.2025.106805

56. Li Y-N, Tao H, Hong J-H, Xiong Y-L, Pan X-C, Liu Y, et al. The Chinese herbal formula huoxiang zhengqi dropping pills prevents acute intestinal injury induced by heatstroke by increasing the expression of claudin-3 in rats. *Evidence-Based Complementary Altern Med*. (2022) 2022:9230341. doi: 10.1155/2022/9230341

57. Karadeniz Cerit K, Koyuncuoğlu T, Yağmur D, Peker Eyüboğlu İ, Şirvancı S, Akkiprik M, et al. Nesfatin-1 ameliorates oxidative bowel injury in rats with necrotizing enterocolitis: The role of the microbiota composition and claudin-3 expression. *J Pediatr Surg*. (2020) 55:2797–810. doi: 10.1016/j.jpedsurg.2020.02.025

58. Huang Z-Q, Ye J, Liu J, Sun L-Y, Ong HH, Wei Y-H, et al. Predictive significance of claudin-3 for epithelial barrier dysfunction in chronic rhinosinusitis with nasal polyps. *Allergy Asthma Immunol Res*. (2023) 15:512–25. doi: 10.4168/aair.2023.15.4.512

59. Wang R, Santos JM, Dufour JM, Stephens ER, Miranda JM, Washburn RL, et al. Ginger root extract improves GI health in diabetic rats by improving intestinal integrity and mitochondrial function. *Nutrients*. (2022) 14:4384. doi: 10.3390/nu14204384

60. He B, Bai J, Wu Z. Glucosamine enhances proliferation, barrier, and anti-oxidative functions in porcine trophectoderm cells. *Food Funct*. (2022) 13:4551–61. doi: 10.1039/d1fo04086c

61. Gogola-Mruk J, Marynowicz W, Krawczyk K, Ptak A. Visfatin increases the invasive potential of ovarian granulosa tumor spheroids by reprogramming glucose metabolism. *Reproduction*. (2023) 165:521–31. doi: 10.1530/REP-22-0443

62. Kollmann C, Niklas C, Ernestus K, Hiller GG, Hörner M, Burkard N, et al. The phenotype of necrotizing enterocolitis correlates with distinct changes of intestinal junctional proteins. *Pathol Res Pract*. (2025) 265:155731. doi: 10.1016/j.prp.2024.155731

63. Liang H, Deng J, Luo T, Luo H, Li F, Wu K, et al. Chromatin accessibility reveals potential prognostic value of the peak set associated with smoking history in patients with lung adenocarcinoma. *Heliyon*. (2024) 10:e41006. doi: 10.1016/j.heliyon.2024.e41006

64. Otani T, Nguyen TP, Tokuda S, Sugihara K, Sugawara T, Furuse K, et al. Claudins and JAM-a coordinately regulate tight junction formation and epithelial polarity. *J Cell Biol*. (2019) 218:3372–96. doi: 10.1083/jcb.201812157

65. Nighot P, Ma T. Endocytosis of intestinal tight junction proteins: In time and space. *Inflammation Bowel Dis*. (2021) 27:283–90. doi: 10.1093/ibd/izaa141

66. Stamatovic SM, Johnson AM, Sladojevic N, Keep RF, Andjelkovic AV. Endocytosis of tight junction proteins and the regulation of degradation and recycling. *Ann N Y Acad Sci*. (2017) 1397:54–65. doi: 10.1111/nyas.13346

67. Chatterjee SJ, Halaoui R, McCaffrey L. Apical–basal polarity as a sensor for epithelial homeostasis: A matter of life and death. *Curr Pathobiol Rep*. (2016) 4:99–106. doi: 10.1007/s40139-016-0107-5